Supplement of Atmos. Chem. Phys., 19, 4439–4457, 2019
https://doi.org/10.5194/acp-19-4439-2019-supplement

Atmospheric Chemistry and Physics
Open Access

Supplement of

Effects of urbanization on regional meteorology and air quality in Southern California

Yun Li et al.

Correspondence to: George A. Ban-Weiss (banweiss@usc.edu)

S1. Evaluation of Simulated $PM_{2.5}$ Concentrations

In this section, the evaluation of simulated $PM_{2.5}$ concentrations using observations from both daily and hourly measurements is discussed. Hourly simulated and observed $PM_{2.5}$ concentrations are both averaged to daily mean $PM_{2.5}$ concentrations for this evaluation. Figure S1 shows the comparison between simulated and observed $PM_{2.5}$ concentrations using both daily and hourly measurements. Modelled values fit well with observations from daily measurement (red dots), and lie between 1:2 and 2:1 ratio lines. However, observations derived from hourly measurements are largely underestimated by the model (blue dots) for nearly half of the points. One possible reason is that hourly measurements tend to report higher $PM_{2.5}$ concentrations than daily measurement, as indicated by Figure S2.

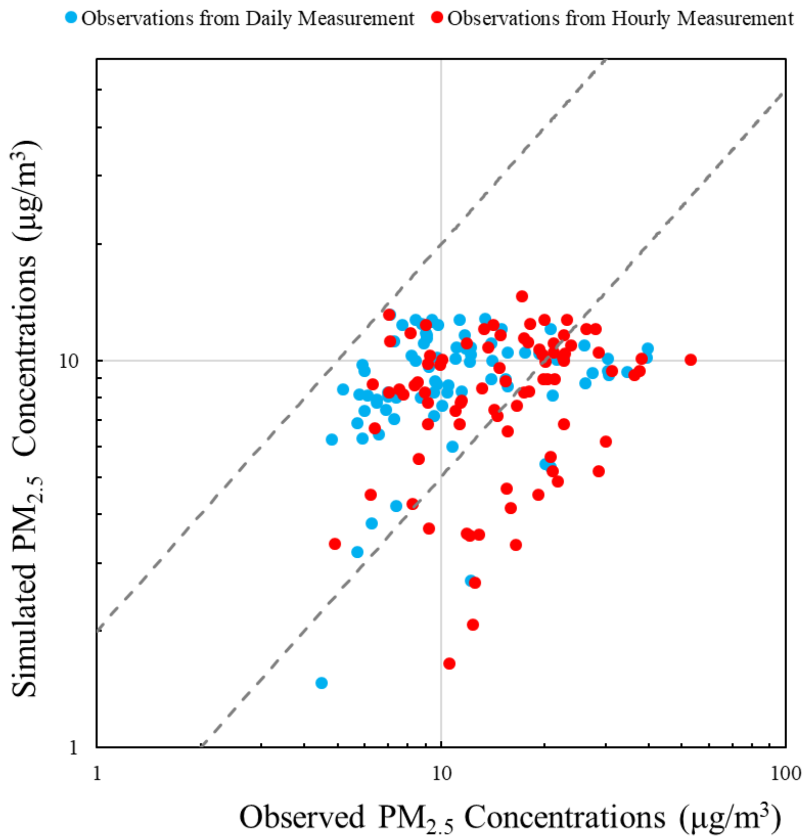

Figure S1. Comparison between modelled and observed PM2.5 concentrations. Observational values from daily gravimetric measurements are shown as blue dots, while red dots show hourly observations using BAMs averaged to daily means. Two dashed grey lines indicate 1:2 and 2:1 ratios between modelled and observed values, respectively.

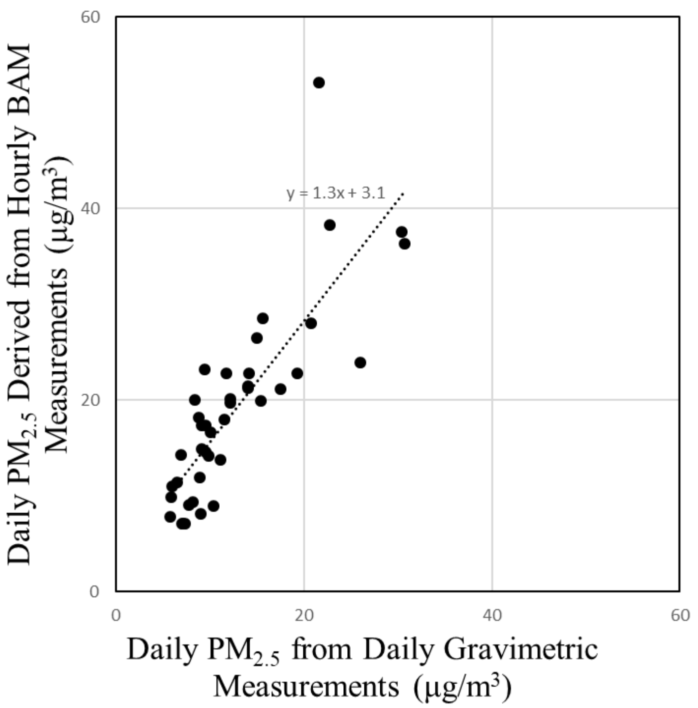

Figure S2. Comparison between collocated daily averaged $PM_{2.5}$ concentrations from daily gravimetric measurements versus hourly BAM measurements.

S2. Detailed Verification of Simulated Near Surface Air Temperature

In this section, we focus on the predicative capability of the model for simulated near-surface air temperature for 1) nonurban sites (shrubs in particular), and 2) differences in urban versus nonurban sites. The data for nonurban observational sites are gathered from MesoWest (https://mesowest.utah.edu/), which are available at Mesonet API (https://developers.synopticdata.com/mesonet/). Figure S3 shows the locations of those nonurban sites. Note that we only use sites that have comparable distance to the sea as the urban sites.

Figure S4 shows the comparison between modeled and observed hourly near-surface air temperature (K) for nonurban sites. In general, the model captures air temperature well at nonurban sites. However, it tends to underestimate observations at relatively low temperature values. Figure S5 shows the time series (Figure S5a) and mean diurnal cycle (Figure S5b) of comparisons between modeled and observed hourly near-surface air temperature (K) for both urban sites and nonurban sites. The model captures the trends in urban / rural differences in air temperature well in general. In the morning, both observed and modeled nonurban sites show slightly higher air temperature than the urban sites, while at night, averaged air temperature at nonurban sites are lower than air temperature at urban sites. These urban – rural differences shown here for Southern California are similar to the results shown in Theeuwes et al. (2015), and have similar trends as the results shown in our paper (Present-day scenario – Nonurban scenario). However, strictly speaking these urban – rural differences should not be interpret as UHI/UCI caused by land surface difference between urban and rural regions. This is because there are many other factors (e.g., distance to the sea) that affect urban – rural differences apart from land surface properties in this region. Finding a good rural reference point for defining the UHI/UCI is thus difficult for the Los Angeles region. This is in part why we study the effects of urbanization in this study as "Present-day" minus "Nonurban," rather than using rural regions outside the city as a proxy for nonurban as is typically done.

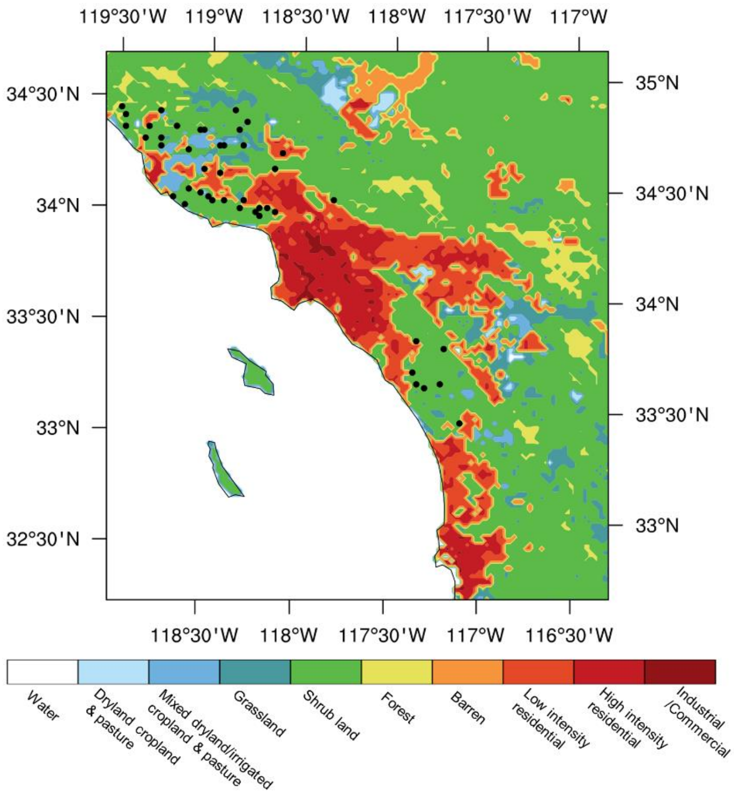

Figure S3. Nonurban observation sites (shown by black dots). The background map shows the land cover types in the Present-day scenario.

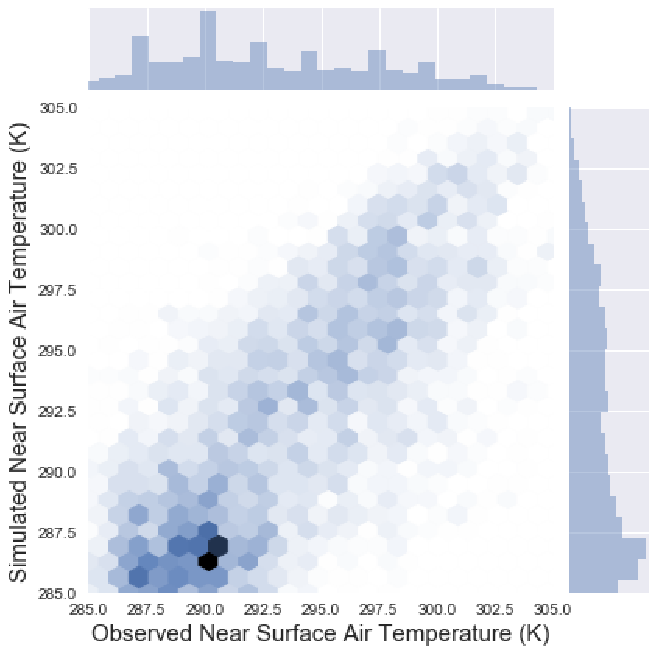

Figure S4. Comparison between modeled and observed hourly near-surface air temperature (K) for nonurban sites that locate at shrub land cover type. Darker hexagonal bins correspond to higher point densities in the scatter plots. Histograms of both observations and modeled values are also shown at the edges of each panel.

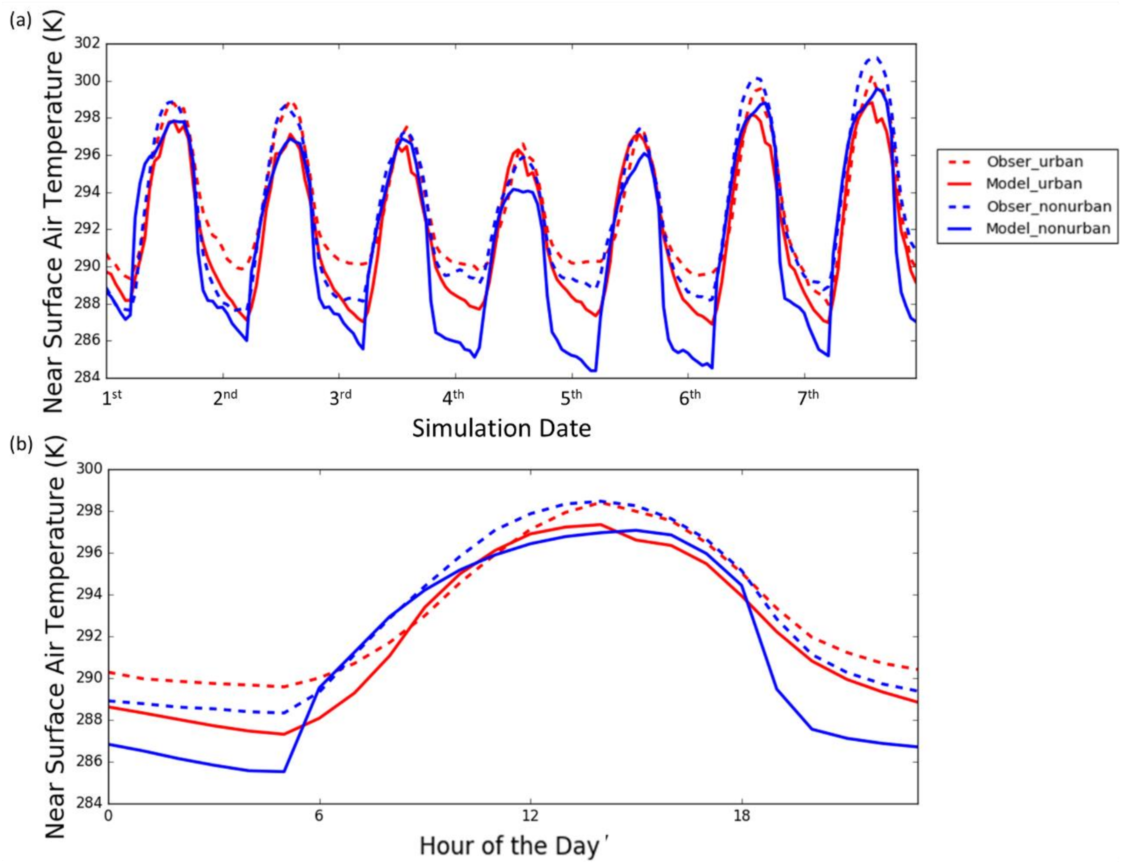

Figure S5 Time series (a) and mean diurnal cycle (b) of modeled and observed hourly near-surface air temperature (K) for both urban sites and nonurban sites. Values in panel (a) are obtained by averaging over urban (nonurban) sites for each simulated hour. Values in panel (b) are obtained by averaging over urban (nonurban) sites and the entire simulation period for each hour of day.

S3. "Present-day No-irrigation" Scenario

In this section, we explain the effects of land surface changes from urbanization but excluding adding irrigation on air temperature. As shown in Figure S6, land surface property changes have led to urban temperature reductions from 8 PST to 15 PST, and increases during other times of day. The largest spatially averaged temperature reduction occurs at 10 PST ($\Delta T = -0.63$ K), whereas the largest temperature increase occurs at 20 PST (+1.3 K). Spatially averaged urban temperature changes during morning, afternoon, and at night are –0.37 K, +0.05 K and +0.72 K, respectively. These changes are significantly different from zero at the 95% confidence level using the paired Student's t-test based on the standard error computed from n=7 daily means.

During the morning, temperature reductions are simulated in most urban regions. However, the magnitude of the reductions is smaller than the difference between the Present-day and Nonurban scenarios (Figure S7a). During the afternoon, most parts of the west LA region and Riverside show increases in air temperature, while air temperature reductions occur in San Fernando Valley (Figure S7b). The pattern shown for inland regions differs from that shown by difference between the Present-day and Nonurban scenarios. During nighttime, temperature increases are larger in the inland regions of the basin than the coastal regions (Figure S7c), which is similar to the pattern shown by Present-day – Nonurban difference.

The aforementioned results indicate that land cover property changes from adopting impervious surfaces (e.g., increases in thermal inertia from the use of manmade materials) can cause air temperature reductions during the day, especially during the morning. However, the magnitude of air temperature reductions is much smaller without including the effects of adding irrigation through urbanization, indicating the important role of irrigation on reducing air temperature.

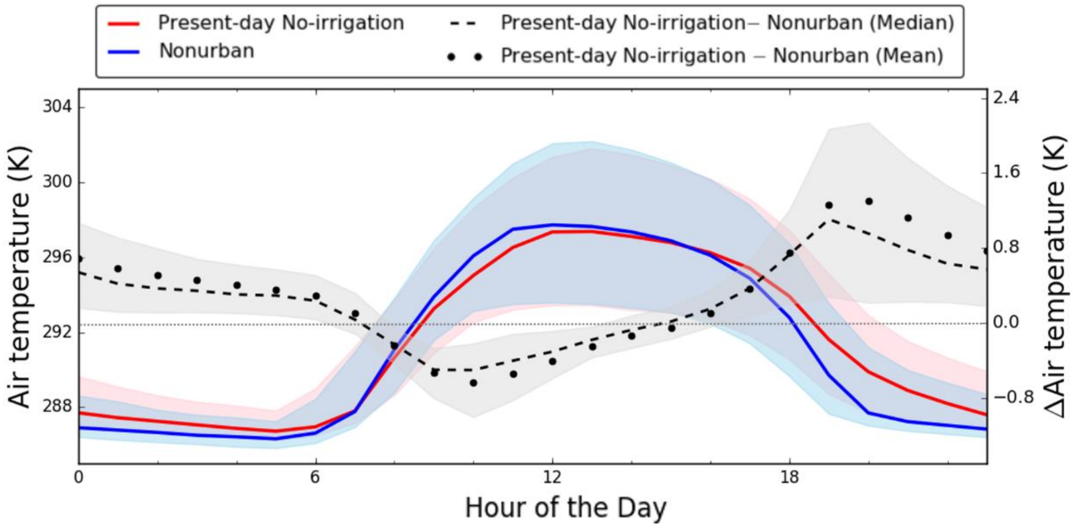

Figure S6. Diurnal cycles for present-day no-irrigation (red), nonurban (blue), and present-day no-irrigation – nonurban (black) for air temperature in the lowest atmospheric layer (K). The solid and dashed curves give the median values, while the shaded bands show 25th and 75th percentiles. Dots indicate mean values for differences between Present-day and nonurban. The horizontal dotted line in light grey shows $\Delta = 0$ as an indicator of positive or negative change by land surface changes via urbanization without involving irrigation.

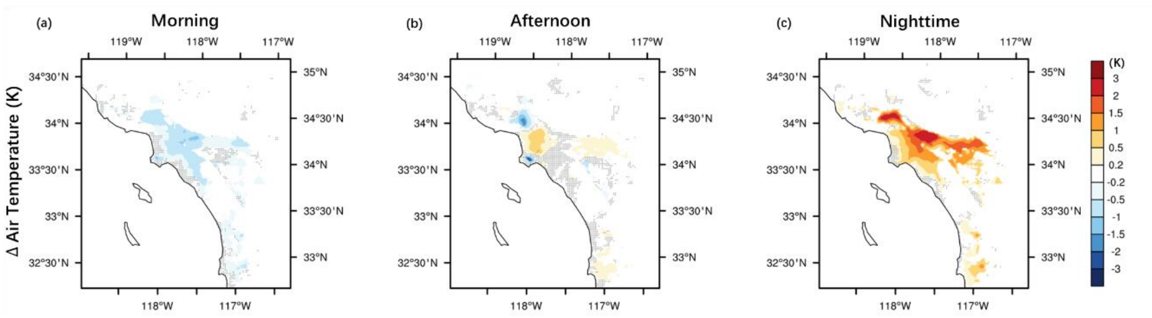

Figure S7. Spatial patterns of differences (Present-day No-irrigation – Nonurban) in temporally averaged values during morning, afternoon and nighttime for air temperature. Note that values are shown only for urban grid cells. Morning is defined as 7 PST to 12 PST, afternoon as 12 PST to 19 PST, and nighttime as 19 PST to 7 PST. Note that values are shown only for urban grid cells. Black dots indicate grid cells where changes are not significantly different from zero at 95% confidence level using the paired Student's t-test with n=7 days.

S4. Other Supplemental Tables and Figures

Table S1. Conversion table from SAPRAC emission to RADM2 emissions. Species abbreviations in SAPRAC, RADM2, weighting factor to apply, and species names are shown

Species in SAPRAC	Species in RADM2	Weighting Factor	Species Name
SO2	E_SO2	1	Sulfur dioxide
NO	E_NO	1	Nitric Oxide
NO2	E_NO2	1	Nitrogen Dioxide
CO	E_CO	1	Carbon monoxide
ALK1	E_ETH	1	Ethane kOH<500 /ppm/min
ALK2	E_HC3	1	Alkane 500<kOH<2500 (exclude C3H8, C2H2, organic acids)
ALK3	E_HC3	1.11	Alkane 2500<kOH<5000 (exclude butanes)
MEOH	E_HC3	0.4	Methanol
ACYE	E_HC3	0.4	Acetylene
ETOH	E_HC3	1.2	Ethanol
ALK4	E_HC5	0.97	Alkane 5000<kOH<10000 (exclude pentanes)
ALK5	E_HC8	1	Alkane kOH>10000
OXYL	E_XYL	1	o-Xylene
PXYL	E_XYL	1	p-Xylene
MXYL	E_XYL	1	m-Xylene
ARO2	E_XYL	1	Aromatic kOH>20000 /ppm/min (exclude xylenes)
B124	E_XYL	1	1,2,4-Trimethyl Benzene
ETHE	E_OL2	1	Ethylene
PRPE	E_OLT	1	Propene
OLE1	E_OLT	1	Alkenes kOH<20000 /ppm/min
MACR	E_OLT	0.5	Methacrolein

(Continue Table.S1)

MVK	E_OLT	0.5	Methyl Vinyl Ketone
ACRO	E_OLT	0.5	Acrolein
IPRD	E_OLT	0.5	Lumped isoprene product species
OLE2	E_OLI	1	Alkenes kOH>20000 /ppm/min
13BDE	E_OLI	1	1,3-Butadienne
BENZ	E_TOL	1	Benzene
ARO1	E_TOL	1	Aromatic kOH<20000 /ppm/min (exclude benzene and toluene)
TOLU	E_TOL	1	Toluene
CRES	E_CSL	1	Cresols
HCHO	E_HCHO	1	Formaldehyde
CCHO	E_ALD	1	Acetaldehyde
RCHO	E_ALD	1	Lumped C3+ aldehydes
BALD	E_ALD	1	Aromatic aldehydes
MACR	E_ALD	0.5	Methacrolein
GLY	E_ALD	1	Glyoxal
MGLY	E_ALD	1	Methyl Glyoxal
BACL	E_ALD	0.5	Biacetyl
ACRO	E_ALD	0.5	Acrolein
IPRD	E_ALD	0.5	Lumped isoprene product species
ACET	E_KET	0.33	Acetone
PRD2	E_KET	1.61	Ketones kOH>7300 /ppm/min
MVK	E_KET	0.5	Methyl Vinyl Ketone
MEK	E_KET	1.61	Ketones kOH<7300 /ppm/min
PACD	E_ORA2	1	Peroxyacetic and higher peroxycarboxylic acids
AACD	E_ORA2	1	Acetic and higher carboxylic acids

(Continue Table.S1)

NH3	E_NH3	1	Ammonia
CH4	E_CH4	1	Methane
PAL	E_PM25I/E_PM25J	0.2/0.8	Primary metal $PM_{2.5}$ – nuclei model and accumulation mode
PCA	E_PM25I/E_PM25J	0.2/0.8	
PFE	E_PM25I/E_PM25J	0.2/0.8	
PK	E_PM25I/E_PM25J	0.2/0.8	
PMG	E_PM25I/E_PM25J	0.2/0.8	
PMN	E_PM25I/E_PM25J	0.2/0.8	
PMOTHR	E_PM25I/E_PM25J	0.2/0.8	
PSI	E_PM25I/E_PM25J	0.2/0.8	
PTI	E_PM25I/E_PM25J	0.2/0.8	
PMC	E_PM_10	1	Unspeciated Primary PM_{10} – nuclei model and accumulation mode
PEC	E_ECI/E_ECJ	0.2/0.8	Elemental Carbon $PM_{2.5}$ – nuclei model and accumulation mode
POC	E_ORGI/E_ORGJ	0.2/0.8	Organic $PM_{2.5}$ – nuclei model and accumulation mode
PSO4	E_SO4I/E_SO4J	0.2/0.8	Sulfate $PM_{2.5}$ – nuclei model and accumulation mode
SULF	E_SO4I/E_SO4j	19.2/76.8	Sulfate $PM_{2.5}$ from sulfates – nuclei model and accumulation mode
PNO3	E_NO3I/E_NO3J	0.2/0.8	Nitrate $PM_{2.5}$ – nuclei model and accumulation mode

Table S2. Model evaluation of the "Present-day" simulation and recommended model performance benchmarks.

Variable	Metrics	Recommended benchmark	Evaluation Result	Reference for recommended benchmark
Hourly near surface air temperature (K)	ME	2 K	1.9 K	(Dean, 2015)
Hourly Ozone concentration (ppb)	NMB	30%	31%	(Emery et al., 2017)
Daily $PM_{2.5}$ concentration ($\mu g/m^3$)	NMB	15%	22%	(Emery et al., 2017)

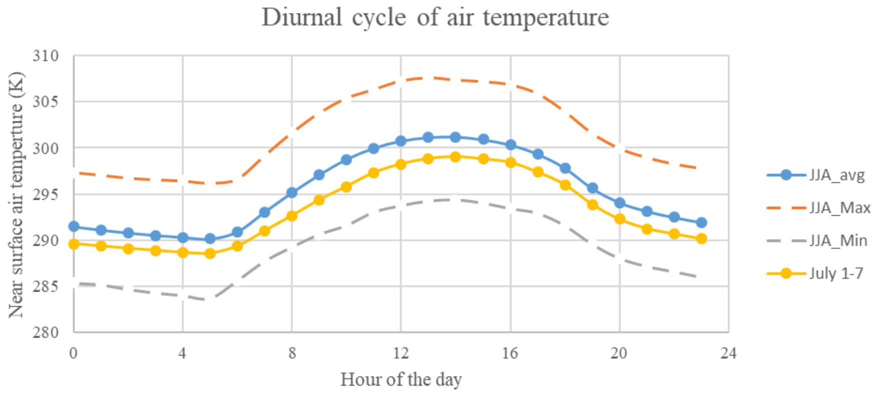

Figure S8. Diurnal cycles for observed near surface air temperature (K) over JJA (June, July and August in year 2012) in blue, and over our simulation period in yellow. Observations are obtained from MesoWest (https://mesowest.utah.edu/), which are available at Mesonet API (https://developers.synopticdata.com/mesonet/). Mean values are derived by averaging over all observational sites available for the innermost domain and the aforementioned period for each hour of day. Orange and grey curves show the maximum and minimum air temperature at each hour of the day for JJA. Results show that our simulation period (July 1-7) is representative of summertime meteorology for our domain.

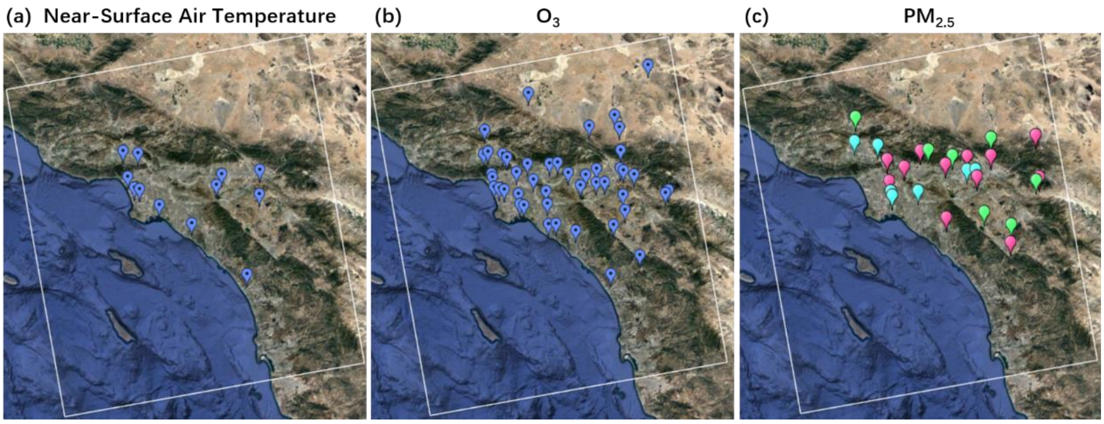

Figure S9. Locations of monitoring stations for (a) near-surface air temperature, (b) O_3 and (c) $PM_{2.5}$ concentration observations. Green, red and blue points in panel c show the locations for stations where only daily observations, only hourly observations, or both daily and hourly observations available, respectively. White solid lines in each panel give the boundary of the innermost (d03) model domain.

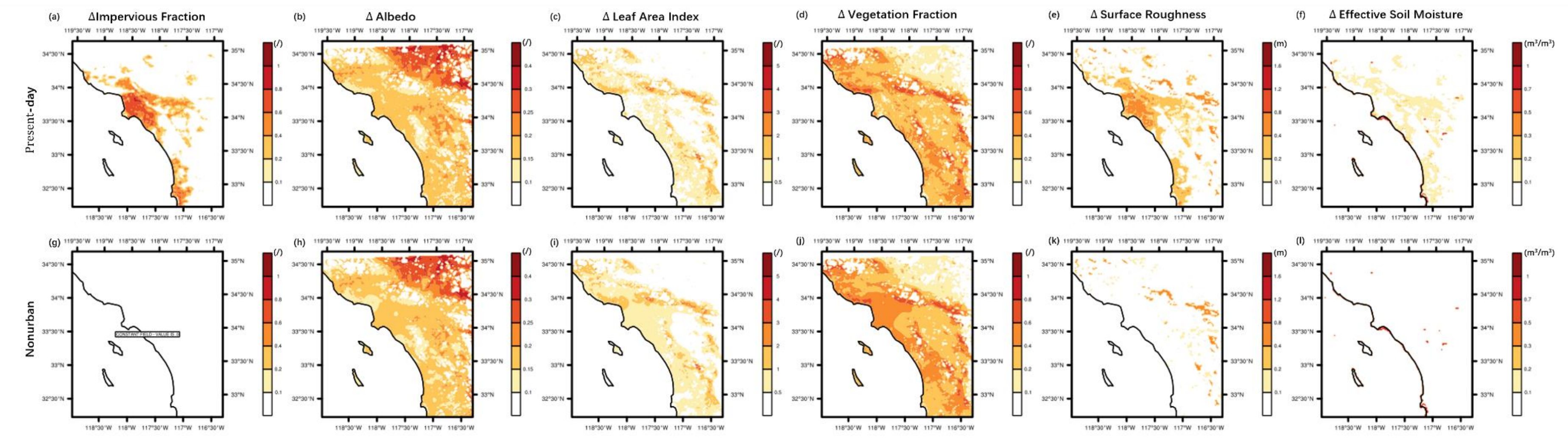

Figure S10. Land surface properties in the Present-day scenario and the Nonurban scenario.

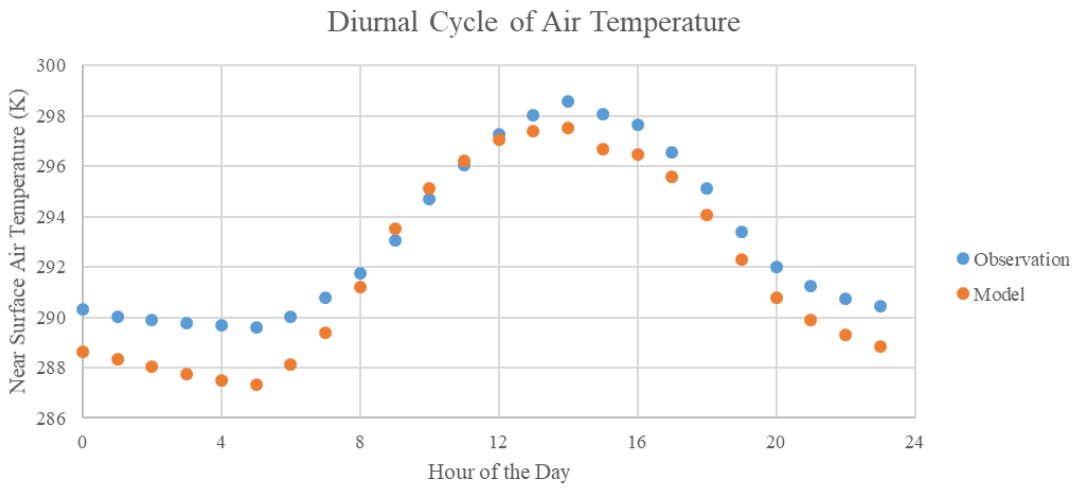

Figure 11. Diurnal cycles for observed and modeled near surface air temperature (K).

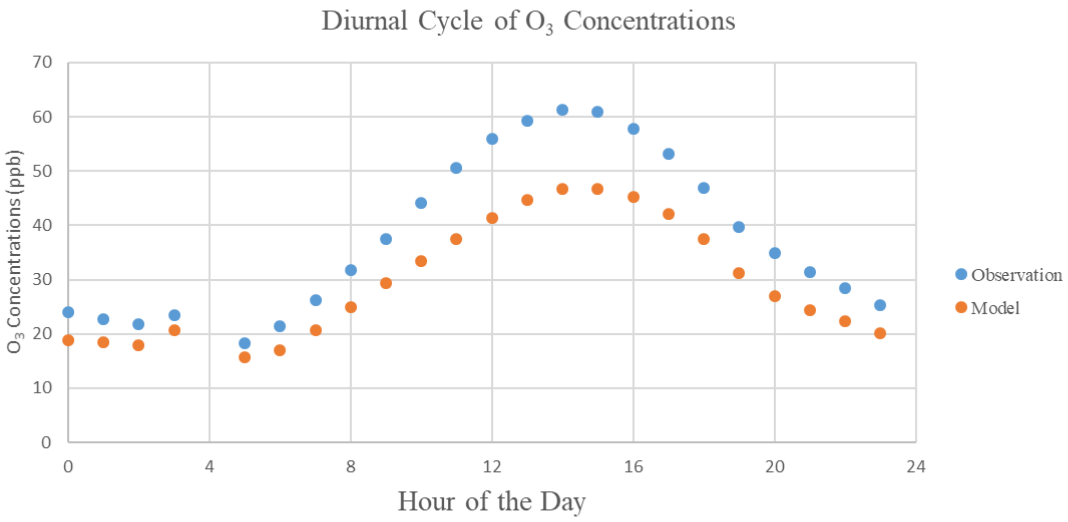

Figure 12. Diurnal cycles for observed and modeled O_3 concentrations (ppb).

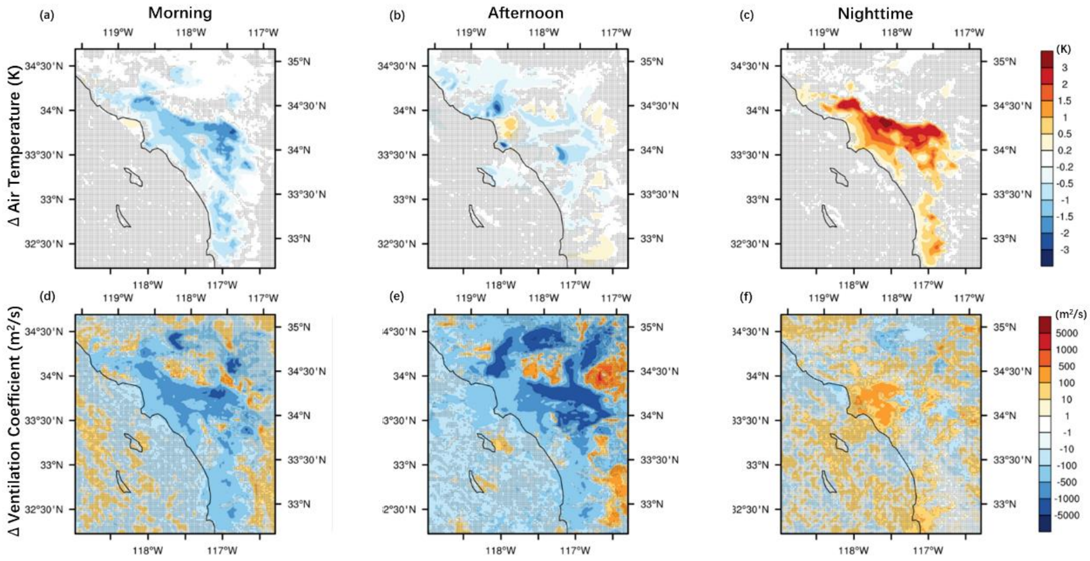

Figure S13. Spatial patterns of differences (Present-day – nonurban) in temporally averaged values during morning, afternoon and nighttime for air temperature in the lowest atmospheric layer, and ventilation coefficient. Black dots indicate grid cells where changes are not significantly different from zero at 95% confidence level using the paired Student's t-test with n=7 days. Morning is defined as 7 PST to 12 PST, afternoon as 12 PST to 19 PST, and nighttime as 19 PST to 7 PST. Values are shown only for the whole innermost domain.

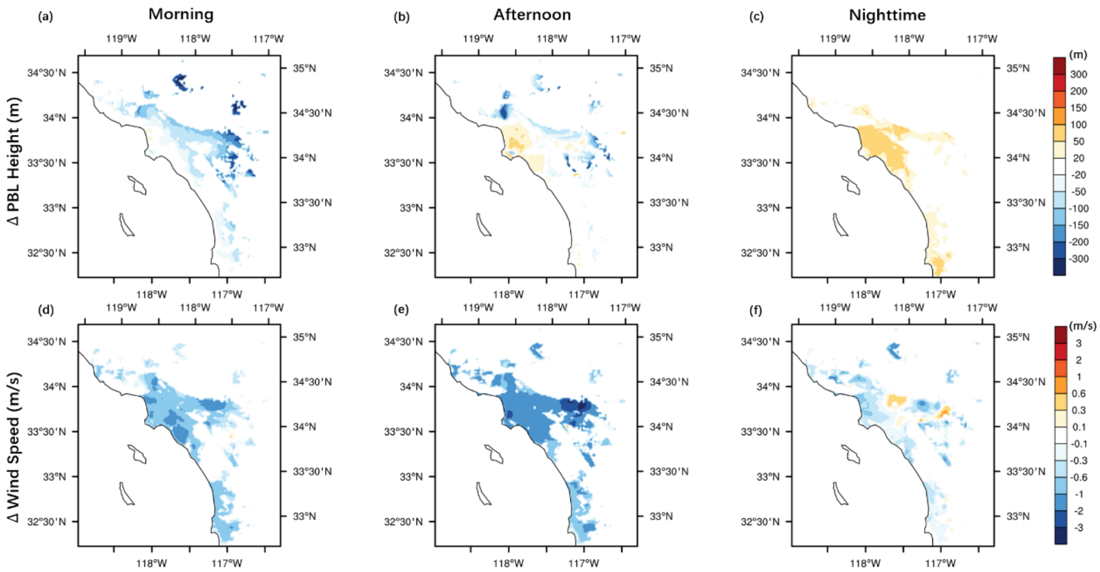

Figure S14. Spatial patterns of differences (Present-day – nonurban) in temporally averaged values during morning, afternoon and nighttime for (a,b,c) PBL heights, and (d,e,f) averaged wind speed under within PBL. Note that values are shown only for urban grid cells. Morning is defined as 7 PST to 12 PST, afternoon as 12 PST to 19 PST, and nighttime as 19 PST to 7 PST. Note that values are shown only for urban grid cells.

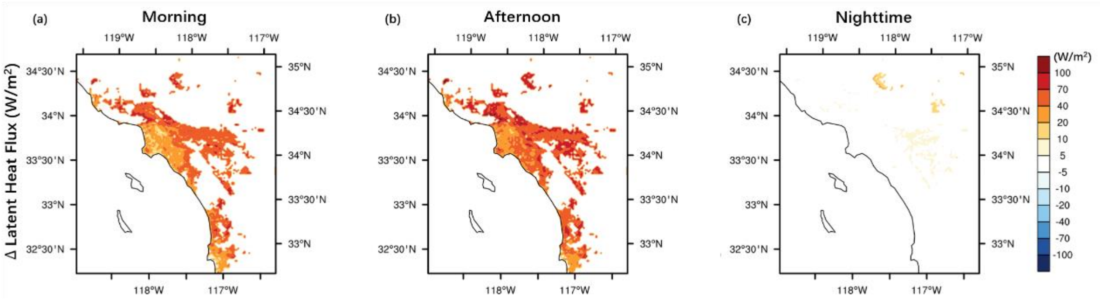

Figure S15. Spatial patterns of differences (Present-day – nonurban) in temporally averaged values during morning, afternoon and nighttime for latent heat fluxes. Note that values are shown only for urban grid cells. Morning is defined as 7 PST to 12 PST, afternoon as 12 PST to 19 PST, and nighttime as 19 PST to 7 PST. Note that values are shown only for urban grid cells.

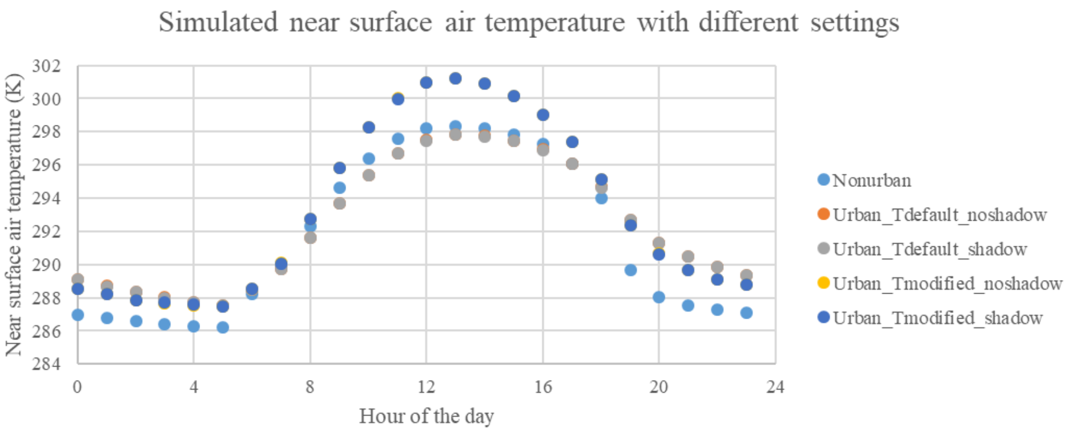

Figure S16. Diurnal cycle of near surface air temperature simulated with different model set-ups. “Tdefault” indicates that the simulation uses the default calculation of surface temperature in WRF, while “Tmodified” indicates that the simulation uses the calculation of surface temperature from Li and Bou-Zeid (2014) (which is also used in (Vahmani el al. (2016)). Dots for “Urban_Tdefault_shadow” and “Urban_Tdefault_noshadow” (“Urban_Tmodified_shadow” and “Urban_Tmodified_noshadow”) are overlapping at every hour of the day because the simulation results with shadow on/off are very similar.

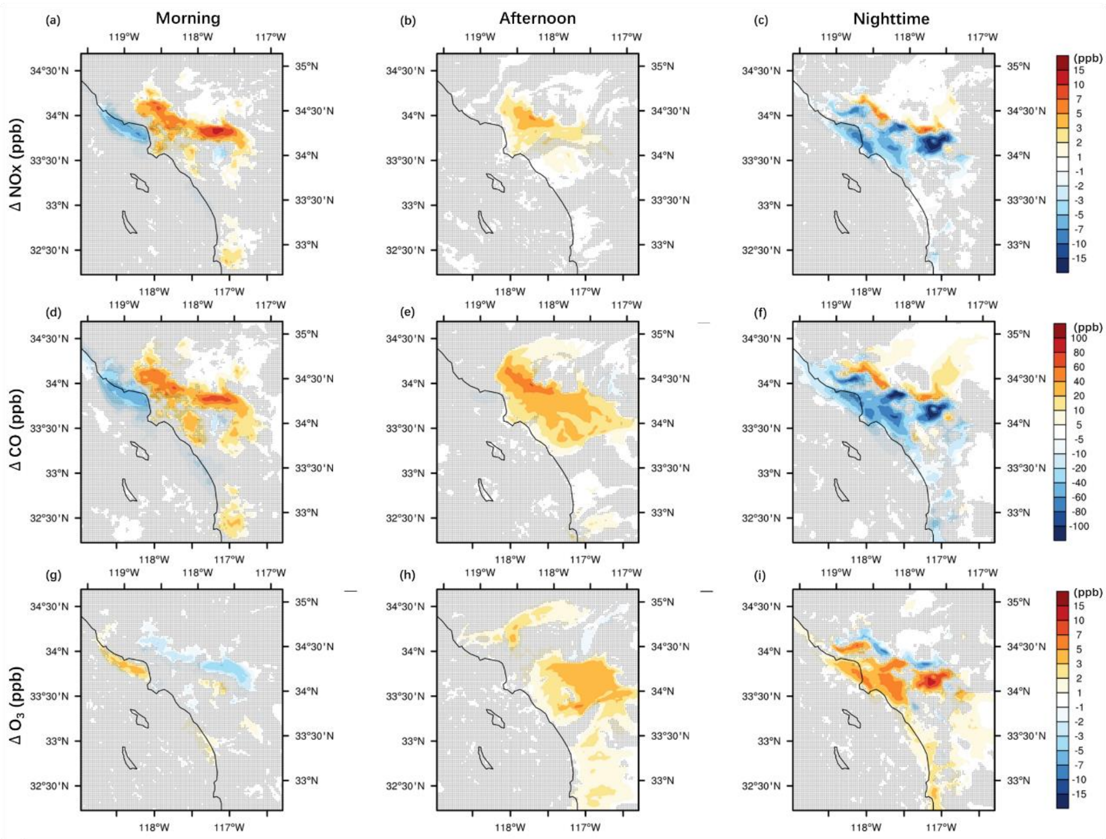

Figure S17. Spatial patterns in differences (Present-day – nonurban) of temporally averaged values during morning, afternoon and nighttime for (a,b,c) NOx, (d,e,f) CO, and (g,h,i) O_3 concentrations. Black dots indicate grid cells where changes are not significantly different from zero at 95% confidence level using the paired Student's t-test with n=7 days. Morning is defined as 7 PST to 12 PST, afternoon as 12 PST to 19 PST, and nighttime as 19 PST to 7 PST.

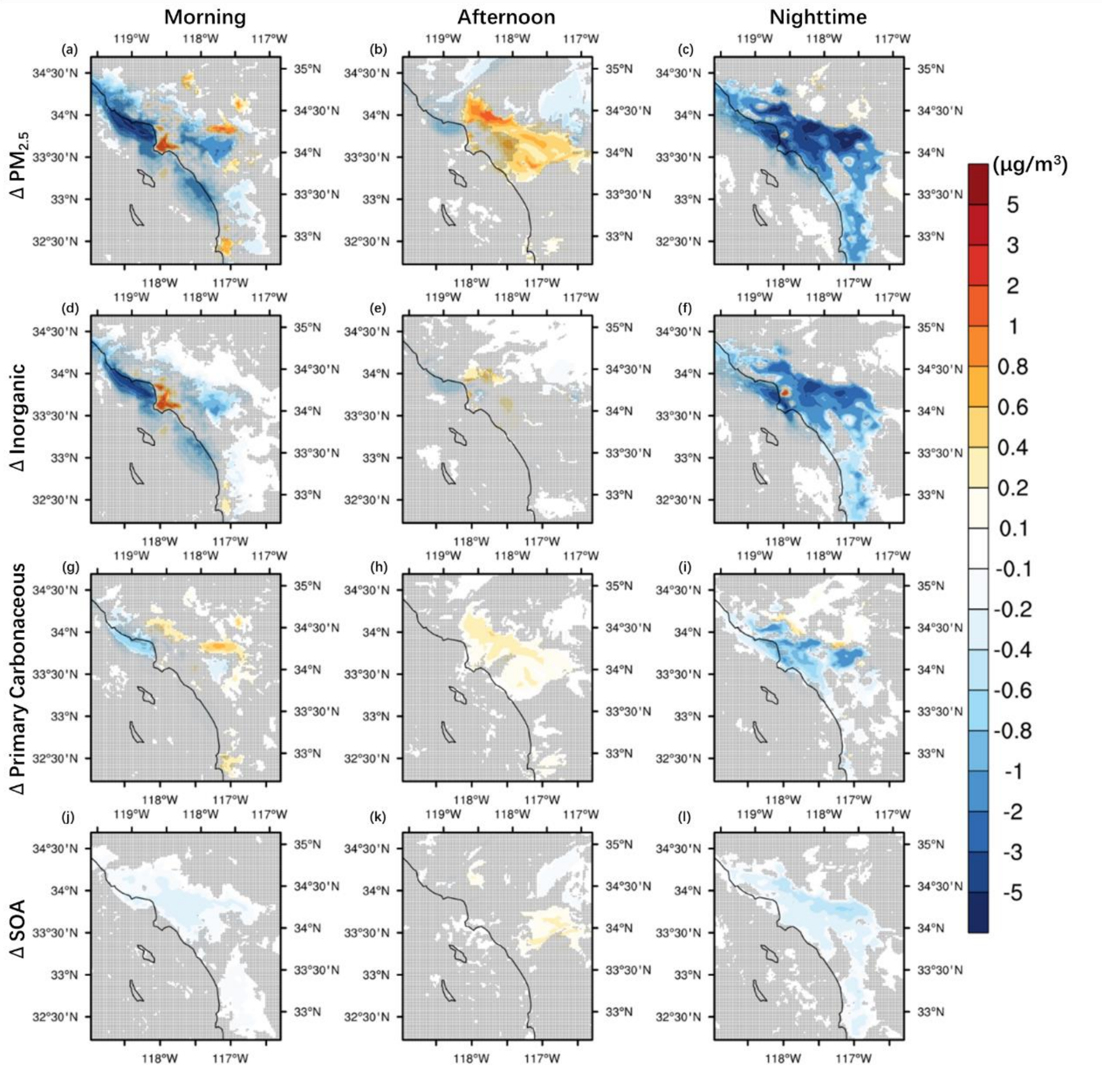

Figure 18. Spatial patterns in differences (Present-day – nonurban) of temporally averaged values during morning, afternoon, and nighttime for $PM_{2.5}$. Panels (a)–(c) show total $PM_{2.5}$; (d)–(f) inorganic aerosol; (g)–(i) primary carbonaceous aerosol; and (j)–(l) secondary organic aerosol. Black dots indicate grid cells where changes are not significantly different from zero at 95% confidence level using the paired Student's t-test with n=7 days. Morning is defined as 7 PST to 12 PST, afternoon as 12 PST to 19 PST, and nighttime as 19 PST to 7 PST.

Reference

Dean, W.: Creating and mapping an Urban Heat Island Index for California FINAL REPORT, available at: https://calepa.ca.gov/wp-content/uploads/sites/6/2016/10/UrbanHeat-Report-Report.pdf, 2015.

Emery, C., Liu, Z., Russell, A. G., Odman, M. T., Yarwood, G., and Kumar, N.: Waste management association recommendations on statistics and benchmarks to assess photochemical model performance, J. Air Waste Ma., 67(5), 582-598, 2017.

Li, D. and Bou-Zeid, E.: Quality and sensitivity of high-resolution numerical simulation of urban heat islands. Environ. Res. Lett., *9*(5), 055001, 2014.

Theeuwes, N. E., Steeneveld, G.-J., Ronda, R. J., Rotach, M. W. and Holtslag, A. A. M.: Cool city mornings by urban heat. Environ. Res. Lett., 10(11), 114022, 2015.

Vahmani, P., Sun, F., Hall, A. and Ban-Weiss, G.:Investigating the climate impacts of urbanization and the potential for cool roofs to counter future climate change in Southern California. Environ. Res. Lett., *11*(12), 124027, 2016.